On the Degradation of InGaAsP/InP-Based Bulk Lasers

Thomas Kallstenius, Jakob Bäckström, Ulf Smith, and Björn Stoltz

***Abstract*— Degradation of InGaAsP/InP-based buried-heterostructure bulk (BH-bulk) lasers has been studied by means of electroluminescence (EL), photoluminescence (PL), electron-beam-induced current (EBIC) and transmission electron microscopy (TEM). Lasers with p/n as well as semi-insulating (SI) current-blocking layers were studied. The results show that moderate increases in the threshold current correlate well with formation of dark defects (DD's) (i.e., dark-line defects (DLD's) or dark-spot defects (DSD's), which cannot be distinguished in our case due to the narrowness of the laser stripe.) The DD's were found to be caused by dislocation loops. The dependence of threshold current increase on the number of DD's is explained in terms of a model which includes effects due to the DD's, as well as changes in the regions outside the DD's. The latter is found to be responsible for the major part of the threshold current increase. Values for the ratio between the carrier lifetimes inside and outside the DD's are presented, for the first time. In our lasers, strong degradation differs from moderate degradation in that DD's do not form during aging. The presence of dislocation loops only at the sidewalls of the active stripe in lasers with p/n current-blocking layers points to the sidewalls as being critical. The near absence of dislocation loops and the smaller increase in threshold current in SI lasers which have degraded strongly, compared to the strongly degrading p/n lasers, suggest that strong degradation is a synergistic combination of damage in the sidewalls and Zn indiffusion from the current-blocking layers.**

***Index Terms*— Degradation, dislocation, electroluminescence (EL), electron beam-induced current (EBIC), InP, laser, photoluminescence (PL), transmission electron microscopy (TEM).**

I. Introduction

BURIED-HETEROSTRUCTURE (BH) InGaAsP/InP-based laser diodes (LD's) are widely used as light sources in high-speed terrestrial and undersea optical communication systems operating in the optical fiber window, 1.0–1.7 μm. In such systems, the reliability of the LD is a crucial factor. Device failure can lead to serious system downtime and high repair costs, so the reliability of the LD's weighs heavily in the system specifications.

Although the use of LD's with multiple quantum-wells (MQW's) grows rapidly, bulk lasers without an MQW-structure are still key components in many present day fiber-optics systems. Therefore the reliability issues concerning such LD's are still important. Furthermore, the simpler bulk structure is ideal for studies of reliability problems in connection with the BH-structure itself, since it is the same in bulk and MQW lasers. Consequently, a proper understanding of the degradation in bulk lasers is important also for MQW-lasers.

The microstructure in degraded InGaAsP/InP-based bulk lasers, as well as the associated DLD's and DSD's, has been the subject of several studies over the years [1]–[4]. Most of these studies involve lasers with p/n current-blocking layers and many authors have attributed the degradation to Zn diffusion from the p-InP:Zn current-blocking layer [5]–[7].

In the present work, a comparison has been made between degradation phenomena in lasers with the same BH but with different current-blocking layers, i.e. p/n and semi-insulating (SI). This is, to our knowledge, the first time such results are presented for SI-lasers. Since such lasers do not have any Zn in the current-blocking layers, degradation due to Zn-diffusion from these layers is not possible. The mechanisms involved in the laser degradation process are elucidated by a detailed collation of the results obtained from macroscopic analyses of the degradation in terms of threshold current and differential external quantum-efficiency, as well as microscopic analyses by EL, PL, EBIC, and TEM. Our results confirm the earlier observations for p/n type lasers and show that although the changes in the microstructure are distinctly different in the two types of lasers, they most likely have the generation of point defects as their common origin. The differences in the microstructure are merely due to the extent of this generation of point defects. A new model is presented for the degradation in threshold current due to the occurrence of DD's and a reduced carrier lifetime outside the DD's. The model allows the ratio between carrier lifetimes inside and outside the DD's to be obtained from the results for the measured degradation in threshold current for the first time.

II. Experimental

InGaAsP/InP-based BH LD's ($\lambda = 1.3$ μm) with SI or p/n current-blocking layers were studied. Two lasers mounted "n-side up" with SI and p/n current-blocking layers, respectively, are shown schematically in Fig. 1(a) and (b). The fabrication of these LD's involved epitaxial growths by means of low-pressure metal-organic vapor-phase epitaxy (LPMOVPE). The LD's were metallized with a triple-layer film, Au/Pt/Ti, on the p-side and Au/TiW or Au/Pt/Ti on the n-side in order to form

Manuscript received March 23, 1999; revised September 10, 1999. This work was supported by Ericsson Components AB, Stockholm, Sweden, and has been performed within the Surface & Micro Structure Technology (SUMMIT) Competence Center (sponsored by the Swedish National Board for Industrial and Technical Development, NUTEK).

T. Kallstenius and U. Smith are with the Materials Science Division, Uppsala University, Uppsala S-75221 Sweden (e-mail: Thomas.Kallstenius@material.uu.se). They are also with the Microelectronics Division, Ericsson Components AB, Stockholm S-16481 Sweden.

J. Bäckström and B. Stoltz are with the Microelectronics Division, Ericsson Components AB, Stockholm S-16481 Sweden.

Publisher Item Identifier S 0733-8724(99)09679-6.

0733–8724/99$10.00 © 1999 IEEE

Authorized licensed use limited to: Univ of Calif Santa Barbara. Downloaded on November 29, 2009 at 10:34 from IEEE Xplore. Restrictions apply.

ohmic contacts. Subsequently, the LD's were mounted onto aluminum nitride subcarriers, using an Au-Sn based solder. For further details regarding the processing, see [8]. In most cases, the LD's were mounted with the n-side up, c.f., Fig. 1. In the EL and PL investigations, this configuration is in general preferable to the p-side up for two reasons. First, the n-side is in general much smoother that the p-side, since the former has been polished before metallization. Artifacts in the EL and PL images due to scattering caused by surface topography are therefore almost completely eliminated in the case of n-side up. Second, the active stripe is only separated from the surface by 1–2 μm for samples mounted p-side up, so any topographic features on the surface will be almost in focus, when the active stripe is imaged during EL. In the case of n-side up, the active stripe is separated from the surface by approximately 100 μm of InP, so the surface will be well out of focus.

LD's from different wafers that had been removed from various production runs due to excessive degradation were studied. Lasers from four wafers with a SI current-blocking layer, hereafter referred to as wafers SI-1 to SI-4, and three wafers with p/n current-blocking layers, i.e. p/n-1 to p/n-3, were studied.

The LD's were stressed by means of accelerated aging. All LD's were aged at a constant current of 150 mA during 50 h at 100°C, a so-called "burn-in" test. Some lasers from wafer SI-1 were then subjected to additional aging at a constant optical output of 3 mW during 4000 h at 70°C, hereafter referred to as a "life-test". The threshold currents and the differential external quantum-efficiencies were evaluated and compared before and after aging. The threshold current was obtained from a linear fit of the light-output power response just above threshold. The differential external quantum-efficiency was compared before and after aging at a fixed current, slightly above the threshold value.

The EL along the active stripe in the LD's was investigated both before and after accelerated aging. For this purpose, the Au/TiW films on the n-side were partly removed by means of selective chemical etching. The LD's were first etched in an Au-stripping solution until the Au-layer was removed. This was followed by a removal of the TiW layer in concentrated H_2O_2 for approximately 15 min. We had no means of removing the Au/Pt/Ti films, so those lasers which had such films on both sides, i.e., p/n-3, could not be studied with EL or PL.

The EL was observed with the aid of an IR-sensitive vidicon mounted on an optical microscope, which had objectives with extra long working distances. The EL from parts of the active stripe was observed at 200, 400 and 1000 times magnification. In order to minimize the signal due to simulated emission at the facets, the LD's were forward biased with an injected current below the threshold level.

Variations in the luminescence along the active stripe were also studied by means of PL mapping. For this, no further sample preparation than that for the EL was necessary. PL mapping was also occasionally used during the preparation of plan-view TEM samples in order to make sure that the preparation did not introduce any artifacts in the sample. This also allowed an exact correlation between features in the PL images and defects observed in the plan-view TEM micrographs. For the PL mapping, a system from ScanTek Inc., France, with a pump lasers ($\lambda = 1018$ nm) was used. This allowed excitation of the active InGaAsP stripe solely, leaving the surrounding InP unaffected, since InP is virtually transparent at this wavelength. The pump laser was focused onto the active InGaAsP stripe by maximizing the PL-intensity output from the stripe. The wavelength corresponding to the PL spectral peak from the active stripe was selected using a grating-based monocromator. For detection of the light signal, an InGaAs-detector with high sensitivity in the 1100–1600 nm range was used. The PL-response was measured along the active stripe using a step size of 0.25 or 1 μm.

In order to obtain further information about the p/n junctions in the lasers, some LD's were also studied by means of the EBIC mode in a scanning electron microscope (SEM). The LD's were connected to an amplifier for detection of the EBIC signal via the subcarrier. A moderately low acceleration voltage, 5 kV, was used, so that the spread of the electron beam in the InP could be kept small without losing too much signal intensity. According to the Kanaya-Okayama expression for maximum electron range [9], this voltage should result in a width of the interaction volume smaller than 0.3 μm.

After the lasers had been studied before and after accelerated aging by means of the methods mentioned above, TEM was used to obtain more information about specific features in the EL and PL images. Both (100) plan-view and (011) cross-section TEM samples of the active region were prepared. For the plan-views, the method of selective chemical-thinning was used. The details of this method are published elsewhere [8]. For the cross-sections, focused-ion-beam (FIB) sample preparation was used, following the technique described by, e.g., Walker *et al.* [10]. The TEM studies were performed using a JEOL 2000FX electron microscope at 200 kV.

III. Results

Our results show that the degradation characteristics for different lasers are essentially the same for all lasers from the same wafer and also that two degradation modes exist.

A. Wafers with Moderately Degrading Lasers

Our criterion for wafers with moderately degrading lasers was an increase in the threshold current of less than 30% for all lasers taken from the same wafer after burn-in. Three wafers with a SI current-blocking layer, i.e. SI-1 to SI-3, and two wafers with p/n current-blocking layers, i.e. p/n-1 and p/n-2, fulfilled this criterion. The change in differential external quantum-efficiency after burn-in was almost undetectable. For the SI lasers which had been subjected to a life-test after burn-in, wafer SI-1, the threshold current and differential external quantum-efficiency changed in a similar manner, although the degradation was lower due to the lower stress level.

Before accelerated aging, the EL was homogenous along the stripe in most samples, as shown in Figs. 2(a) and 3(a). In a few cases, some small dark regions could be observed. The resolution of the EL is limited by the diffusion length of the carriers in InGaAsP, which is about 2 μm [11]. Since this is more than the width of the stripe ($\sim$1 μm), it is not

Authorized licensed use limited to: Univ of Calif Santa Barbara. Downloaded on November 29, 2009 at 10:34 from IEEE Xplore. Restrictions apply.

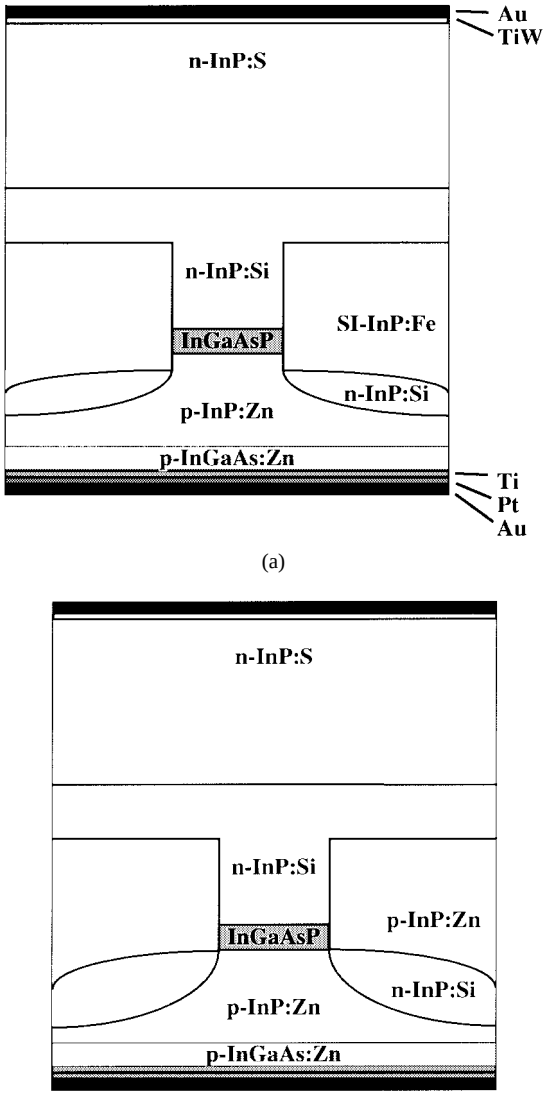

Fig. 1. Outlines of InGaAsP/InP-based BH lasers with (a) a SI current-blocking layer and (b) p/n current-blocking layers, both mounted n-side up.

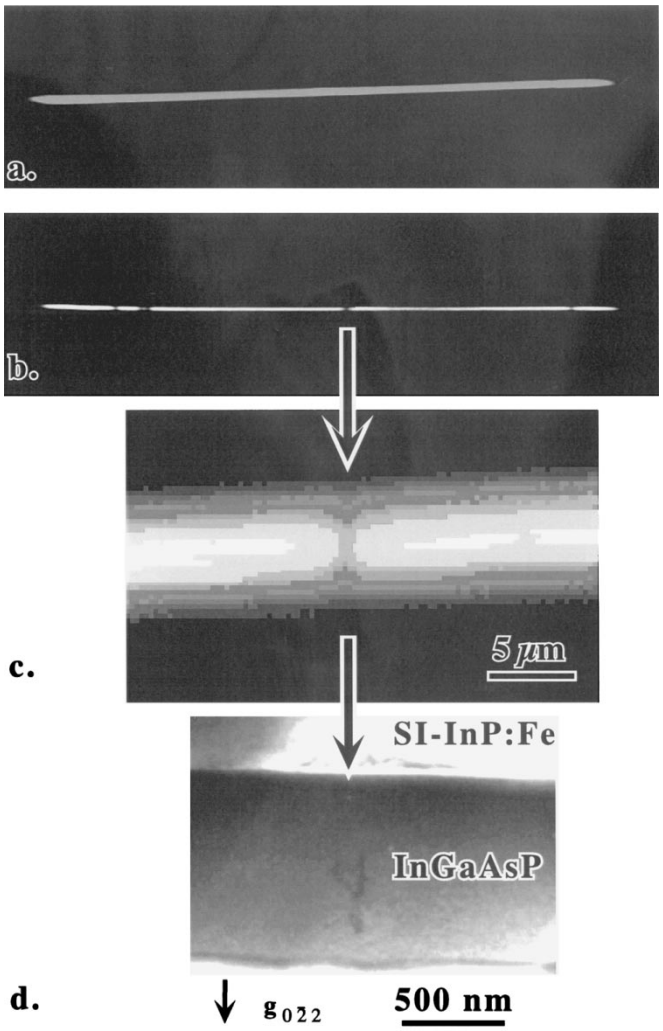

Fig. 2. SI laser from wafer SI-2. The threshold current increased by 13% after burn-in. (a) EL from the active stripe before and (b) after burn-in. (c) PL mapping after burn-in. (d) A plan-view TEM image from the area corresponding to the PL mapping showed that a dislocation loop coincided with the DD.

possible to obtain information about the internal structure of the dark regions. We are, therefore, not able to describe these regions in terms of the established concepts DLD's and DSD's [1]–[3], [12] and will simple refer to them as DD's. After burn-in, DD's showed up in most LD's. For example, several new DD's were found both for the SI laser in Fig. 2(b) and for the p/n laser in Fig. 3(b). These DD's could also be resolved in the PL images, as shown in Fig. 2(c).

For the SI LD's, the threshold current increase vs. the number of DD's is shown in Fig. 4(a). As seen in the Figure, the number of DD's after burn-in is generally larger in LD's showing a large increase in threshold current. This also holds true after the life-test. The same tendency was found for the p/n lasers in Fig. 4(b). An overall impression was also that the DD's observed after burn-in in lasers from wafer SI-1 showed increased contrast after the life-test.

The defect structure in the DD's was studied by plan-view TEM. The plan-view TEM micrograph of the SI laser in Fig. 2(d) shows that a dislocation loop had developed in the DD. In fact, a closer look at the original negative reveals the presence of an additional small loop just below the larger loop. The size of the bigger loop is approximately 200 nm. The sample preparation technique used [8] leaves the active stripe unaffected and due to the thickness of this stripe, i.e., $\sim$150 nm, the Burger's vector, $\mathbf{b}$, of the loops could not be determined unambiguously. The loops were visible for $\mathbf{g} = \pm[0\bar{2}2]$, where $\mathbf{g}$ is the diffraction vector, whereas only residual contrast was obtained for $\mathbf{g} = \pm[022]$. Considering the $\mathbf{g} \cdot \mathbf{b} = 0$ and $\mathbf{g} \cdot \mathbf{b} \times \mathbf{u} \neq 0$ criteria for residual contrast, where $\mathbf{u}$ is a unit vector along the dislocation line, this implies that $\mathbf{b}$ is $\pm a/2[0\bar{1}1]$, $\pm a/3[1\bar{1}1]$ or $\pm a/3[\bar{1}\bar{1}1]$.

The DD's also coincided with dislocation loops in the p/n laser in Fig. 3. Fig. 3(c) shows a dislocation loop-pair, which coincides with one of the DD's in Fig. 3(b). The size of these loops is about 200 nm and the presence of residual contrast for $\mathbf{g} = \pm[0\bar{2}2]$ suggests that $\mathbf{b}$ is $\pm a/2[011]$, $\pm a/3[111]$ or $\pm a/3[\bar{1}11]$.

Authorized licensed use limited to: Univ of Calif Santa Barbara. Downloaded on November 29, 2009 at 10:34 from IEEE Xplore. Restrictions apply.

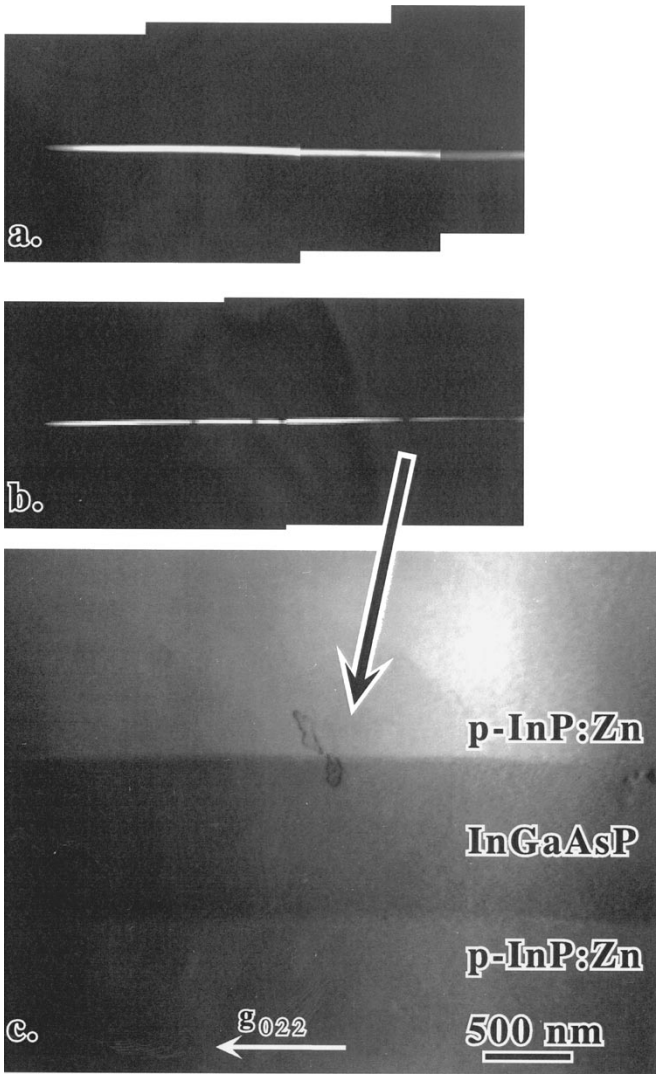

Fig. 3. The p/n laser from wafer p/n-2. The threshold current increased by 8% after burn-in. (a) EL from the active stripe before and (b) after burn-in. (c) A plan-view TEM image from the same area of the active stripe showing that a DD coincided with a dislocation loop pair with a starting point in the sidewalls of the active stripe.

All observed loops appear to coincide with DD's. The loops are closed and are not linked to any other crystal defects. In fact, no evidence of other crystal defects whatsoever was found in our TEM samples. It is interesting to notice that the loop in the SI laser in Fig. 2(d) is located near the center of the stripe rather than at the sidewalls, whereas both dislocation loops in the p/n laser in Fig. 3(c) have their starting point at the sidewall. One of the latter loops has grown into the active InGaAsP layer and the other into the p-InP:Zn current-blocking layer.

B. Wafers with Strongly Degrading Lasers

Our criterion for wafers with strongly degrading lasers was an increase in the threshold current of more than 30% after burn-in for at least some lasers from one and the same wafer. Two different wafers, one with a SI current-blocking layer (SI-4) and one with p/n current-blocking layers (p/n-3), fulfilled this criterion. Since the degradation characteristics for these

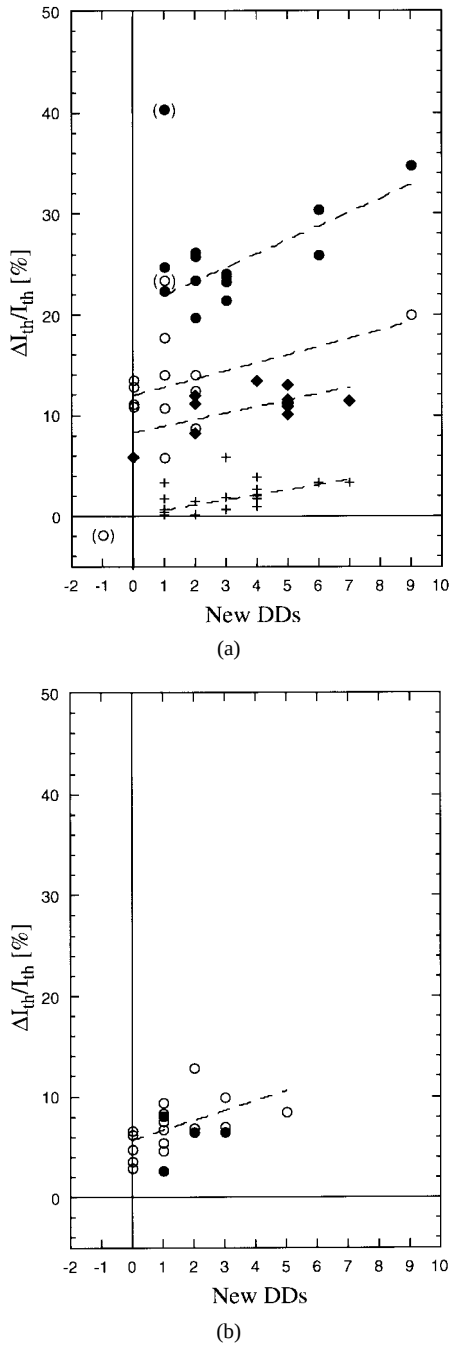

Fig. 4. Increase in threshold current versus increase in number of DD's in lasers from different wafers with (a) a SI current-blocking layer and (b) p/n current-blocking layers. The data points within brackets in (a) were omitted in the calculations (see text for details). The results of the calculations and the symbols used in the graphs are listed in Table I. The dashed lines represent averages taken in the high density regions of data points and are only intended to guide the eye.

wafers had apparent distinctions, we have chosen to present the results for each wafer separately.

1) Lasers with SI Current-Blocking: The distribution in threshold current increase after burn-in was quite broad for the lasers from SI-4 when compared to the distribution for lasers with moderate degradation. For the majority of the lasers, the threshold current increase was less than 2% with no measurable change in the differential quantum-efficiency. In addition, about one third of the LD's showed an increase

Authorized licensed use limited to: Univ of Calif Santa Barbara. Downloaded on November 29, 2009 at 10:34 from IEEE Xplore. Restrictions apply.

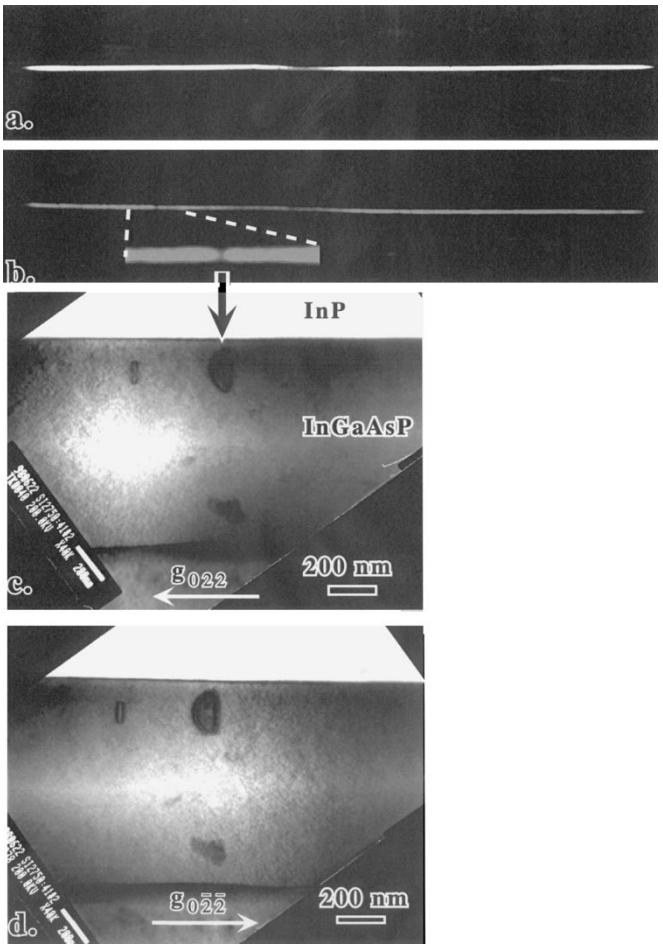

Fig. 5. EL images of a SI-LD from wafer SI-4 (a) before and (b) after burn-in, with an increase in threshold current by 62%. The degradation resulted in an EL image with uneven edges and reduced intensity. Plan-view TEM investigations of the active InGaAsP stripe after burn-in showed that the only DD that existed in this LD, and which existed even before the burn-in, corresponds to a dislocation loop with (c) inside contrast for $\mathbf{g} = [022]$ and (d) outside contrast for $\mathbf{g} = [0\bar{2}\bar{2}]$.

in threshold current in the range from 30 to 200%, with a reduction in differential quantum-efficiency of about one order of a magnitude smaller.

Before burn-in, the EL was homogenous along the stripe in all LD's. A rare exception was the DD in Fig. 5(b), which could also be observed before the burn-in, although it is not resolved in the reproduction in Fig. 5(a). Despite that the threshold current had increased by more than 30% in some LD's after burn-in, no new DD's could be detected in any of the LD's. Instead, a new phenomenon was observed in the form of an unevenness in the EL along the active stripe. This can only barely be seen in the reproduction of the original EL image in Fig. 5(b). The unevenness was only observed in lasers with an increase in threshold current by more than 30%, e.g., in the LD in Fig. 5, which had degraded 62%. An overall impression was also that the EL intensity was reduced to some extent after burn-in. However, it was not possible to quantify this with our equipment.

A plan-view TEM investigation of the LD in Fig. 5 after burn-in showed the active stripe to be almost free from crystal defects. The only exceptions found were the two dislocation loops shown in Fig. 5(c) and (d). These loops appear to be located in the vicinity of the sidewall of the active stripe and their location along the stripe coincides with the only DD in the sample. The presence of residual contrast for $\mathbf{g} = \pm[0\bar{2}2]$ suggests that $\mathbf{b}$ is the same as for the p/n laser in Fig. 3. The nature of the larger loop, i.e., vacancy or interstitial type, could be determined by means of contrast experiments involving stereographic imaging and observations of inside–outside contrast using a positive deviation parameter s and $\pm\mathbf{g}$ bright field (BF) diffraction imaging [13]. In Fig. 5(c) and (d), the inside–outside contrast can be seen in the form of a change in diameter of the loop parallel to the $\mathbf{g}$-vector. From this contrast change, the loop was determined to be of interstitial type. This is consistent with results of several other groups [5], [14], [15].

2) Lasers with p/n Current-Blocking In the lasers from p/n-3, the increase in threshold current varied between 100–500%. Despite this large increase, any change in external differential quantum-efficiency was hardly resolvable. No significant differences could be found in the nonlinearity of the light-output power when compared before and after burn-in. In fact, no apparent change in the nonlinearity after accelerated aging was observed for any of the lasers in this study. Due to the presence of Au/Ti/Pt metallic films on both sides of these LD's, the EL and PL could not be studied. Instead, LD's were examined by means of plan-view and cross-sectional TEM before and after burn-in.

Plan-view TEM investigations showed that in an LD that had not been subjected to burn-in, Fig. 6(a), no crystal defects could be detected in the active stripe. In contrast to this, an LD with a 210% increase in threshold current after burn-in, had small dislocation loops (<100 nm) located inside the active stripe, as shown in Fig. 6(b) and (c). The loops were more of less homogeneously distributed along the stripe and all loops were situated right at the interface to the p-InP:Zn current-blocking layer.

Fig. 7(a) and (b) show cross-sectional TEM images of two LD's, one before and one after burn-in. As seen in Fig. 7(a), the active stripe and the surrounding InP are clearly visible in the LD not subjected to burn-in, but no crystal defects could be observed in any of the layers, except for a contrast deviation at the sidewalls of the mesa. Fig. 7(b) shows that the LD that had been subjected to burn-in had essentially the same features, except for an additional contrast in the form of two black lobes ("coffee-bean" contrast) at each of the sidewalls of the active stripe. In order to illustrate this more clearly, a schematic drawing has been inserted in Fig. 7(b). The contrast looks essentially the same as the contrast from dislocation loops observed by de Cooman *et al.* in degraded double-channel planar BH lasers (DCPBH) [5].

The determination of the Burgers vector for these small dislocation loops is difficult because of the presence of residual contrast. From the TEM cross-section in Fig. 7(b), the loops appear to be located in {111}-planes. Such loops usually have a Burgers vector of the type $(a/3)\langle 111\rangle$ [1]. Such a Burgers vector is, in fact, consistent with a contrast analysis of the loops in plan-view, using different diffraction conditions with the electron beam close to the [100] direction. Residual

Authorized licensed use limited to: Univ of Calif Santa Barbara. Downloaded on November 29, 2009 at 10:34 from IEEE Xplore. Restrictions apply.

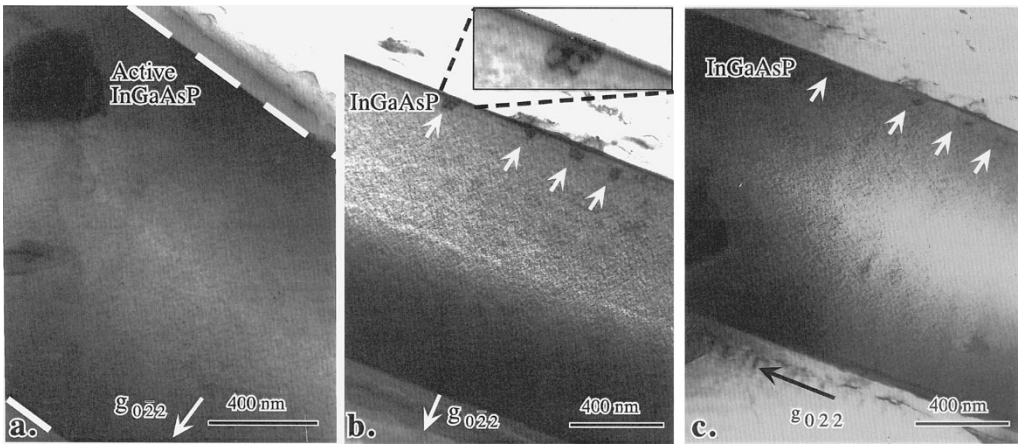

Fig. 6. Plan-view TEM images of the active InGaAsP stripe in p/n-LD's from wafer p/n-3. In (a), an LD that has not been subjected to burn-in is shown. No crystal defects were found. The two dark regions to the left side are artifacts due to the sample preparation. In (b) and (c), the same type of LD is shown after burn-in. The increase in threshold current was 210%. Dislocation loops that are visible at the sidewall of the InGaAsP stripe for (b) $\mathbf{g} = [0\bar{2}2]$ and (c) less visible (residual contrast) for $\mathbf{g} = [022]$.

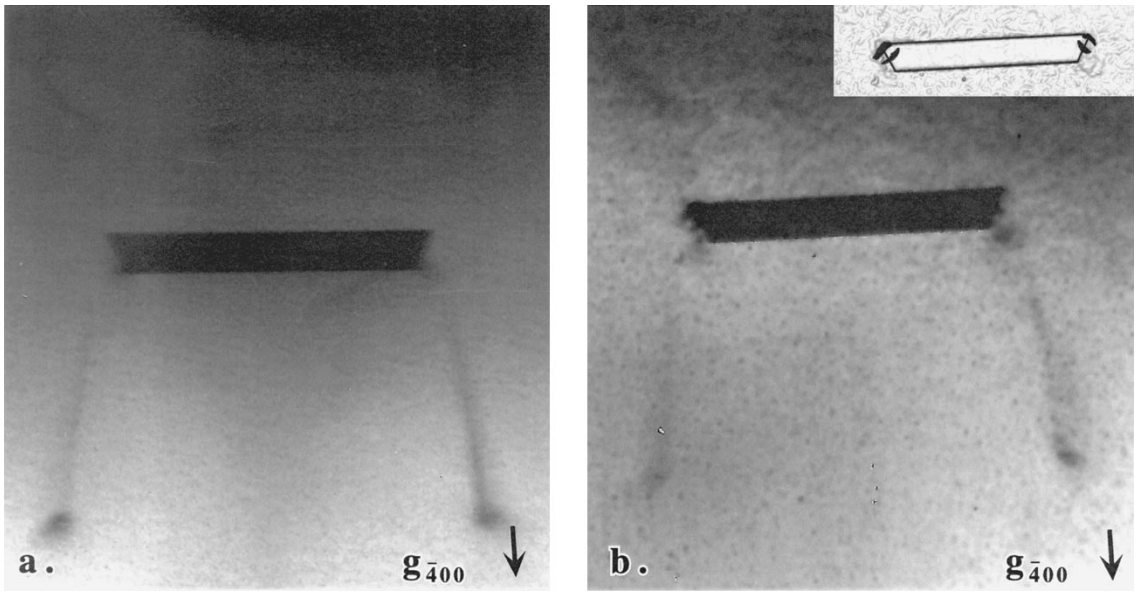

Fig. 7. Cross-sectional TEM of LD's from wafer p/n-3. (a) An LD that has not been subjected to burn-in. (b) An LD after burn-in with an increase in threshold current by 194%. The "coffee-bean"-like contrast observed at the sidewalls of the active stripe is typical for dislocation loops (sketched in the insert).

contrast was only obtained for $\mathbf{g} = \pm[022]$, as shown in Fig. 6(c), which implies that the Burgers vector is $\pm(a/3)[11\bar{1}]$ or $\pm(a/3)[\bar{1}1\bar{1}]$.

In order to study the influence of the dislocation loops on the p/n junctions, some LD's were also studied by means of cross-sectional EBIC before and after burn-in. Results for two different LD's after burn-in are shown in Fig. 8(a) and (b). The increase in threshold current was 286% and 438%, respectively. In the LD of Fig. 8(a), all p/n junctions in the BH-structure are clearly visible, c.f., Fig. 1(b). The widths of the lines in the EBIC image are generally of the order of the diameter of the expected interaction volume for the electron beam, $\sim$0.3 μm and no variations can be seen along the EBIC lines. In Fig. 8(b), on the other hand, there is no EBIC signal right at the interface between active stripe and the p-InP:Zn current-blocking layer, c.f., Fig. 1(b). The absence of an EBIC signal in this part of the structure was also noted before burn-in for some LD's of the same type.

IV. Discussion

A. Wafers with Moderately Degrading Lasers

The majority of the lasers from wafers with moderate degradation showed DD's after burn-in, whereas only occasional DD's were found before aging. Furthermore, the increase in threshold current was found to be related to the increase in the number of DD's, as shown in Fig. 4(a) and (b). This behavior was the same in both SI and p/n lasers.

The presence of DD's in the EL as well as the PL images implies that the DD's correspond to areas of enhanced nonradiative recombination. Therefore, the current density is presumably higher inside the DD's. In addition, the DD's may have a different absorption coefficient compared to the surroundings. We have been able to formulate a model for this degradation in the threshold current. The model includes effects from the DD's, as well as contributions due to changes

Authorized licensed use limited to: Univ of Calif Santa Barbara. Downloaded on November 29, 2009 at 10:34 from IEEE Xplore. Restrictions apply.

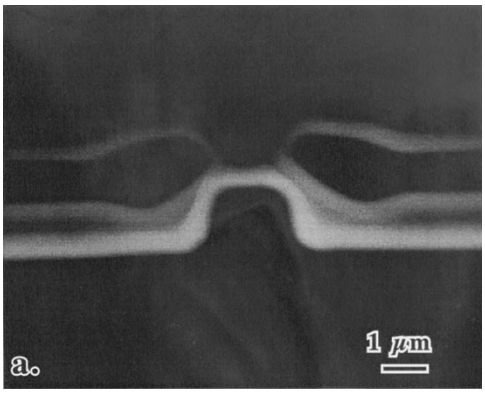

(a)

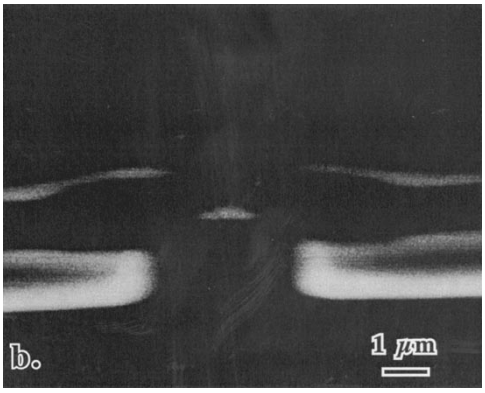

(b)

Fig. 8. EBIC images of two p/n-LD's from wafer p/n-3 after burn-in. (a) LD with an increase in threshold current by 286% and (b) by 438%.

in the carrier lifetime in the regions of the laser stripe outside the DD's.

Following the theory of Yonezu *et al.* [16], the total injected current is divided into two components, one inside the DD's and one inside the normal ("good") regions. Assuming that the current-density in the DD's at threshold, $J_{\rm DD}$, is C times that in the normal regions, $J_{G,\rm th}$,

$$J_{\rm DD} = J_{G,\rm th} \cdot C \tag{1}$$

the total current-density $J_{\rm th}$ can be expressed in the following form [16]:

$$J_{\rm th} = \left[1 + (C-1)\frac{w_{\rm DD}}{L} \cdot n_{\rm DDs}\right] \cdot J_{G,\rm th} \tag{2}$$

where $n_{\rm DDs}$ is the number of DD's, $w_{\rm DD}$ is the effective width of a DD and L is the length of the laser stripe. $w_{\rm DD}$ is expected to be of the order of the carrier diffusion length in InGaAsP, which is around 2 μm [11].

The part of the threshold current which is injected into the normal regions, $I_{G,\rm th}$, can be expressed in terms of the electron charge, q, the volume, V_G, the carrier lifetime, τ_G, and the threshold carrier-density, $N_{G,\rm th}$ [4]:

$$I_{G,\rm th} = \frac{q \cdot V_G \cdot N_{G,\rm th}}{\tau_G} \tag{3}$$

It follows from (2) and (3) that the total threshold-current, $I_{\rm th}$, can be written as:

$$I_{\rm th} = \frac{q \cdot V \cdot N_{G,\rm th}}{\tau_G} \cdot \left[1 + (C-1)\frac{w_{\rm DD}}{L} \cdot n_{\rm DDs}\right] \tag{4}$$

where V is the volume of the entire active stripe.

Eliseev *et al.* [17] have shown how inhomogeneities in the current distribution depend on inhomogeneities in the surrounding material. In accordance with their theory, we now introduce a "current self-distribution parameter," $\xi_{\rm DD}$, which includes the response of the Fermi voltage to changes in carrier density, excess carrier lifetime, specific resistivity and characteristic lengths related to current lines through the DD's [17]. Since $C-1$, according to the definition in (1), is equal to $(J_{\rm DD} - J_{G,\rm th})/J_{G,\rm th}$, a direct application of (20) in Eliseev *et al.* [17] gives

$$(C-1) = -\left(\frac{\Delta\tau_{\rm DD}}{\tau_{\rm DD}}\right) \cdot \frac{\xi_{\rm DD}}{1+\xi_{\rm DD}} \tag{5}$$

Here, $\tau_{\rm DD}$ is the carrier lifetime inside the DD and $\Delta\tau_{\rm DD} = \tau_{\rm DD} - \tau_G$. $\xi_{\rm DD}$ is given by [17]

$$\xi_{\rm DD} = \left(\frac{dU_j}{dN}\right)_{\rm average} \cdot \frac{8 \cdot \tau_{\rm DD}}{(\rho_p + \rho_n) \cdot q \cdot \pi \cdot w_{\rm DD} \cdot d_A} \tag{6}$$

where U_j is the junction voltage, ρ_p and ρ_n are the resistivities in the adjacent p- and n-InP layers, respectively, and d_A is the thickness of the active InGaAsP stripe. We have assumed that $w_{\rm DD}$ is much smaller than the thicknesses of the adjacent p- and n-InP layers.

The $N_{G,\rm th}$ factor in (4) can be obtained from the threshold requirement for the optical field. Assuming a linear gain, $g(N) = a(N - N_0)$, where a is the gain coefficient and N_0 the transparency carrier density, this can be expressed as [18]

$$\begin{aligned}&\Gamma_{xy} \cdot a \cdot (N_{G,\rm th} - N_0) \cdot L \\ &\quad = \alpha_G \cdot (L - L_{\rm DDs}) + \alpha_{\rm DDs} \cdot L_{\rm DDs} + \alpha_m \cdot L\end{aligned} \tag{7}$$

where Γ_{xy} is the transverse confinement factor, α_G is the internal loss in the normal regions, $\alpha_{\rm DDs}$ is the loss in the DD's and α_m is the mirror loss.

By combining (4), (5) and (7), a relation between the increase in threshold current and the number of DD's can be obtained. We assume that the internal losses α_G and $\alpha_{\rm DDs}$ are mainly due to free-carrier absorption and thus proportional to N. Losses due to scattering can either be included in the $\alpha_m \cdot L$-term or be neglected if they are due to the DD's, for which $w_{\rm DD} \ll L$. Neglecting second-order terms, the relation takes the following form:

$$\begin{aligned}\frac{\Delta I_{\rm th}}{I_{\rm th}} &= \left(-\frac{\Delta\tau_G}{\tau_{G0}}\right) \\ &\quad + \left(1 - \frac{\alpha_G}{\xi_{\rm DD} \cdot (N_0 \cdot \Gamma_{xy} \cdot a + \alpha_G + \alpha_m)}\left(\frac{\tau_{\rm DD}}{\tau_G}\right)\right) \\ &\quad \times \left(1 - \frac{\Delta\tau_G}{\tau_{G0}}\right)\left(\frac{\xi_{\rm DD}}{1+\xi_{\rm DD}}\right)\left(\frac{\tau_G}{\tau_{\rm DD}} - 1\right) \\ &\quad \cdot \left(\frac{w_{\rm DD}}{L}\right) \cdot n_{\rm DDs}.\end{aligned} \tag{8}$$

The carrier lifetimes $\tau_{\rm DD}$ and τ_G in (8) are determined by the lifetimes for the different recombination processes below

Authorized licensed use limited to: Univ of Calif Santa Barbara. Downloaded on November 29, 2009 at 10:34 from IEEE Xplore. Restrictions apply.

TABLE I
$\tau_{\rm DD}/\tau_G$ AND C VALUES AS WELL AS AVERAGE VALUES OF $\Delta\tau_G/\tau_{G0}$ FOR WAFERS WITH MODERATELY DEGRADING LASERS

Wafer	Aging	$[\Delta\tau_G/\tau_{G0}]_{\rm average}$	$\tau_{\rm DD}/\tau_G$	C	Figure(s)
SI-1	Burn-in	-11%	0.4	2.1	4a: O
SI-1	Burn-in and life-test	- 22 %	0.3	2.7	4a: ●
SI-2	Burn-in	- 8 %	0.5	1.9	4a: ♦
SI-3	Burn-in	-1%	0.6	1.6	4a: +
p/n-1	Burn-in	- 6 %	0.3	2.5	4b: O
p/n-2	Burn-in	-	-	-	4b: ●

threshold: spontaneous and nonradiative. $\Delta\tau_G$ is expected to arise from changes in the nonradiative lifetime during aging. This is most likely caused by point defects in the active stripe, which form nonradiative recombination centers [19]. Since these point defects are unintentional from a manufacturing point-of-view, their number is likely to fluctuate from laser to laser, which will be reflected in a statistical distribution in the lifetime and, consequently, in $\Delta I_{\rm th}/I_{\rm th}$.

$\xi_{\rm DD}$ can be estimated with the help of (6) for our 1.3 μm InGaAsP/InP lasers, where $d_A = 0.15$ μm and $L = 300$ μm. For $\tau_{\rm DD}$, we use a typical value, 2 ns [20]. From this and the threshold currents, $N_{G,\rm th}$ was estimated to be about $2 \cdot 10^{18}$ cm^{-3}, which gives $\xi_{\rm DD} \approx 3.5$. Using this value together with the approximate values $\alpha_G = 20$ cm^{-1} and $\alpha_m = 40$ cm^{-1} [4] and assuming that $\tau_{\rm DD} \leq \tau_G$, (8) can be approximated by

$$\frac{\Delta I_{\rm th}}{I_{\rm th}} = \left(-\frac{\Delta\tau_G}{\tau_{G0}}\right) + \left(1 - \frac{\Delta\tau_G}{\tau_{G0}}\right)\left(\frac{\xi_{\rm DD}}{1+\xi_{\rm DD}}\right)\left(\frac{\tau_G}{\tau_{\rm DD}} - 1\right) \cdot \left(\frac{w_{\rm DD}}{L}\right) \cdot n_{\rm DDs}. \quad (9)$$

The ratio $\tau_G/\Delta\tau_{\rm DD}$ is expected to be approximately the same for all lasers from the same wafer.

Equation (9) represents a linear relationship between $\Delta I_{\rm th}/I_{\rm th}$ and $n_{\rm DDs}$ and has been used to evaluate the data in Fig. 4. For a given wafer and a given slope of the line (and thus a given ratio $\tau_G/\tau_{\rm DD}$) we have first let the line pass through each of the data points in turn. From this, we have obtained the corresponding $\Delta\tau_G/\tau_{G0}$ for each point. The slope was then varied until the smallest standard deviation for the distribution of $\Delta\tau_G/\tau_{G0}$ values was obtained for each wafer. The data points within brackets in Fig. 4(a) were excluded in the evaluation, since they gave rise to distorted $\Delta\tau_G/\tau_{G0}$ distributions and abnormally large standard deviations. Also, removing the data point near 40% for wafer SI-1 after burn-in plus life-test caused $\tau_{\rm DD}/\tau_G$ to go from 0.4 to 0.3. The corresponding value after burn-in only was 0.4. This implies an increased nonuniformity within the laser after the life-test, which is more consistent with our observation that the DD's showed an enhanced contrast after the life-test. The data point within brackets in the third quadrant in Fig. 4(a) showed a behavior different from all the others and was not included in the fitting. This data point is discussed further below. The data points represented by black dots in Fig. 4(b) belong to wafer p/n-2. Although they show a behavior similar to that of the data points from p/n-1 in Fig. 4(b), they were considered too few in number to allow a meaningful evaluation.

The evaluated ratios of $\tau_{\rm DD}/\tau_G$ and the averages for the $\Delta\tau_G/\tau_{G0}$ distributions are shown in Table I. The corresponding $\Delta\tau_G/\tau_{G0}$ histograms are shown in Fig. 9. According to Table I, the lifetime inside a DD is only about half of that outside. As mentioned above, the observed increase in the contrast in the EL images from lasers after the life-test is consistent with a further reduction of the nonradiative lifetime inside the DD's, c.f., $\tau_{\rm DD}/\tau_G$ for SI-1 after burn-in and life-test. Fig. 4 shows that the degradation is dominated by the change in τ_G, since the slope of the lines representing the contributions from the DD's is quite small. This is not surprising if one considers the change in τ_G to be due to the injection or creation of point defects and the change in $\tau_{\rm DD}$ to be due to dislocations. It is reasonable to expect the creation of point defects to take place over quite a large part of the active stripe, whereas effects due to dislocations are limited to the dislocations themselves and their immediate vicinity. The fact that $[\Delta\tau_G/\tau_{G0}]_{\rm average}$ has changed from -11% after burn-in to -22% after life-test for SI-1 in Table I is consistent with a model in which there is a continuous supply of point defects during aging. Furthermore, the increased number of lasers with large $n_{\rm DD's}$-values after life-test indicates that when the concentration of point defects becomes large in some part of the active region, they agglomerate and form dislocation loops, which are then seen as DD's in the EL and PL images.

Although occurring only at one instance in our experiments, the disappearance of one DD after burn-in for wafer SI-1 is consistent in the sense that it is accompanied by a corresponding reduction in $I_{\rm th}$, c.f., Fig. 4(a). This leads one to raise the question whether point defects are annihilated as well as DD's. In fact, the change in $-\Delta\tau_G/\tau_{G0}$ is slightly negative for some lasers from SI-3, c.f., Fig. 9(a), which makes it likely that annihilation of point defects also occurs. However, in most cases it is swamped by a larger contribution from the creation of new defects.

The C values for the wafers were also calculated, using (5). As seen from Table I, they fall in the range 1.6 to 2.7. Interestingly, these values are of the same order as the corresponding values reported for AlGaAs/GaAs-based lasers by Yonezu *et al.* [16], who obtained $C \approx 2$, in an experiment similar to ours and by Kobayashi *et al.* [21], who obtained the value 2 using thermal diagnosis of DD's. This implies that the influence of DD's on the injected carriers is almost the same in AlGaAs/GaAs and InGaAsP/InP-based lasers. However, a smaller size of the DD's in the latter case makes the presence of DD's less severe.

The wafers used in our investigations are wafers that have been removed from various production runs due to their showing exceptionally large levels of degradation. It is interesting to note that all the lasers from the same wafer degrade about equally much, c.f., Figs. 4 and 9. Since the stress conditions were the same for all lasers, this implies that the source of point defects was built into the wafer at some, presently unknown, stage of the manufacturing process. The identity of the point defects involved as well as the physical mechanism behind the formation of DD's are presently not clear. The fact that the DD's were found to coincide with dislocation loops in both SI and p/n lasers suggests that the mechanism is the same in both types of lasers. Several authors have attributed the formation of dislocation loops in the active

Authorized licensed use limited to: Univ of Calif Santa Barbara. Downloaded on November 29, 2009 at 10:34 from IEEE Xplore. Restrictions apply.

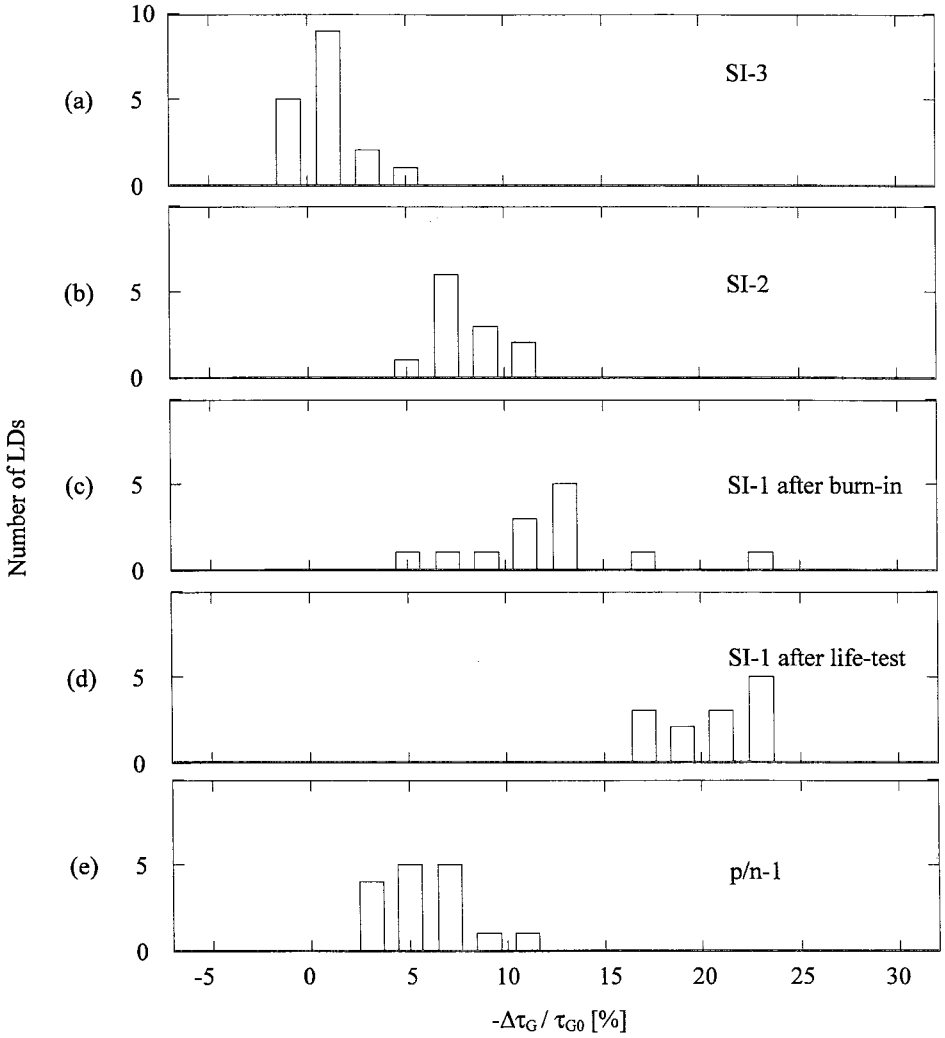

Fig. 9. Histograms showing the distributions in $\Delta\tau_G/\tau_{G0}$ for wafers with moderately degrading lasers.

InGaAsP stripe to Zn diffusion from the layers adjacent to the active stripe [5], [6]. In our lasers, one of the faces of the stripe is, in fact, in contact with a fairly large source, viz. the p-InP:Zn contact layer, as seen in Fig. 1. In the case of p/n lasers, Zn diffusion from the p-InP:Zn current-blocking layer through the sidewalls of the stripe is also possible, c.f., Fig. 1(b). Consequently, loops caused by Zn indiffusion at the sidewalls of the active stripe should only be possible in p/n-lasers but not in SI-lasers. In view of this, it is interesting that the dislocation loop in the SI laser in Fig. 2(d) is located toward the center line of the active stripe, whereas the dislocation loops in the p/n laser of Fig. 3(c) have starting points at the sidewall. It appears as if the sites for the formation of dislocations are governed by the strongest source of Zn, with the sidewalls taking precedence in the p/n type lasers. Not only is the concentration of Zn higher in the p/n current-blocking layer, the sidewalls may also contain some residual damage due to, e.g., phosphor deficiency or from the reactive ion etching (RIE) steps. This is discussed more in detail in the next section.

B. Wafers with Strongly Degrading Lasers

In the SI-LD's, which degraded strongly, a certain degree of unevenness could be observed along the entire stripe after burn-in in the EL images. This is different from the moderately degrading lasers and suggests that some type of highly localized defects exist along the stripe. Although dislocation loops were the exception rather than the rule in these SI lasers, the location of the few loops in the active stripe was the same as for the large number of loops in strongly degraded p/n lasers, i.e., at the sidewall. In the latter case, numerous small dislocation loops showed up after burn-in, as seen in Figs. 6 and 7, which suggests that the formation of the loops is strongly related to the structural and chemical conditions at the sidewalls.

The missing EBIC signal after burn-in in regions corresponding to the sidewalls of the active stripe in Fig. 8(b) coincides with the presence of dislocation loops in that area. The EBIC signal originates in the depletion regions of the p/n junctions [22] and an absent EBIC signal suggests that the carrier recombination rate is enhanced in these regions. de Cooman *et al.* [5] have observed a similar phenomenon and they attribute the EBIC effects at the sidewalls of their lasers to the presence of dislocation loops of the same type as ours. In view of this, it is interesting to note that lasers with the same EBIC pattern could be found before burn-in as well, whereas dislocation loops were only found after burn-in. Judging from

Authorized licensed use limited to: Univ of Calif Santa Barbara. Downloaded on November 29, 2009 at 10:34 from IEEE Xplore. Restrictions apply.

this, there seems to exist small and highly localized defects in the sidewalls of the active stripe already before the burn-in. The defects may be due to an inadequate removal of the sidewall damage in these lasers during processing. Further evidence for the presence of damaged sidewalls is the contrast deviation at the mesa sidewalls seen both before and after burn-in in Fig. 7.

The relative increase in threshold current was considerably larger than the reduction in external differential quantum efficiency. This implies a negligible change in the internal absorption. Therefore, the dislocation loops and any defects in the sidewalls of the active stripe act as sinks for the injected carriers by forming strong nonradiative recombination centers, which is consistent with the EBIC result.

Hence, it appears as if the strong degradation has its origin in some type of damage at the sidewalls of the active stripe. Furthermore, the observed lower threshold current increase in the SI lasers (0–200%) compared to the p/n lasers (100–500%) shows that the concentration of point defects is lower in the SI lasers. This is consistent with the fact that these lasers do not have a Zn-doped current-blocking layer adjacent to the defect ridden sidewalls of the active region. It also relates well to out observation of the numerous small loops in the p/n lasers, since de Cooman *et al.* have suggested that such loops are caused by Zn diffusion [5]. Wittorf *et al.* [23] have also attributed interstitial loops in the Zn-diffused region of InP to an agglomeration of In interstitials, which are generated by a kick-out reaction when diffusing Zn interstitials are incorporated on the In sublattice.

We therefore suggest that the strong degradation in some of our p/n lasers is a synergistic effect caused by residual damage at the sidewalls of the active stripe in combination with Zn diffusion from the current-blocking layer. It has been shown earlier that Zn diffusion into the active InGaAsP stripe generated nonradiative recombination centers [7]. Anomalously large Zn diffusion from the current-blocking layer into the mesa due to dry-etch damage has been reported by Kondo *et al.* [24]. Oohashi *et al.* [25] have increased the lifetime of their lasers by the insertion of a diffusion barrier for Zn in the form of an undoped InP layer next to the mesa sidewalls.

C. Relationship Between Moderate and Strong Degradation

The results presented above enable us to draw some conclusions regarding the relationship between the groups "Wafers with Moderately Degrading Lasers" and "Wafers with Strongly Degrading Lasers." However, it is important to note that the occurrence of moderately or strongly degrading lasers are sporadic effects and should be considered as being due to perturbations in an otherwise very stable production process. The overwhelming majority of lasers do not show any measurable degree of degradation. The two groups differ not only in terms of the degree of degradation, as displayed by the change in I_{th}, they also show distinct microstructural differences. The strongly degraded lasers of p/n type have a large number of small dislocation loops right at the sidewalls, whereas the moderately degraded ones have dislocations in DD's inside the active region. In the strongly degraded SI-type lasers, on the other hand, no dislocations could be observed, apart from some occasional dislocation inside the active region. However, the unevenness in the intensity of the EL radiation, taken together with the absence of dislocations, indicates that there must at least exist some residual damage at the sidewalls. This damage is large enough to affect the recombination rate, but not large enough to generate dislocations. In the moderately degraded SI lasers, dislocations were found at the DD's, as was the case with the p/n-type lasers.

In view of this, we interpret the groups "strong," "moderate," and "no degradation" as representing various degrees of residual damage at the sidewalls of the mesa. Probable causes of such damage are inadequate removal of process-induced defects, such as defects from the reactive-ion etching steps and also the presence of defects related to an uncontrollable loss of, e.g., phosphorous atoms from the mesa sidewalls during regrowth of the epilayers. When the amount of residual damage is large, strong sites for nonradiative recombination or current-leakage develop right at the sidewalls of the active region. When the amount is moderate, such sites develop inside the active region. The location of the sites depends on the extent to which point defects are able to enter the active region. Thus, damage at the sidewalls should not only be able to generate point defects; it should also encourage local nucleation and growth of dislocations, if strong enough. This will absorb point defects and prevent them from entering the bulk of the active region. The fact that the strongly degraded p/n-type lasers show dislocation loops which have developed enough to be resolvable in the TEM also shows that when a Zn-doped layer is present, it will cooperate with the residual damage and cause an even stronger injection of point defects.

V. Conclusions

The analysis of degraded InGaAsP/InP-based bulk lasers resulted in the following conclusions:

In our lasers, moderate degradation in InGaAsP/InP-based BH lasers is connected with the appearance of DD's (DLD's or DSD's) in the EL images. These DD's are caused by the presence of dislocation loops. DD's were found in lasers both with p/n and SI current-blocking structures. Differences in the location of the loops point to indiffusion of Zn as being of importance in the creation of the dislocations.

An analytical model is proposed in which the DD's and part of the increase in the threshold current are due to nonuniformities in the current distribution caused by the presence of dislocations. A comparison of the model with experimental results showed the carrier lifetime in the DD's to be about half of that in regions outside the DD's. This is, to our knowledge, the first time quantitative estimations of this ratio have been presented. The model also shows that the contribution due to changes in the carrier lifetime in those parts of the laser stripe which do not have DD's is responsible for the major part of the increase in threshold current. The influence from the DD's plays only a minor role. The former is most likely caused by the presence of point defects which form nonradiative recombination centers during aging.

Authorized licensed use limited to: Univ of Calif Santa Barbara. Downloaded on November 29, 2009 at 10:34 from IEEE Xplore. Restrictions apply.

Strong degradation was found to be different from moderate degradation in that DD's are not formed in this case. The presence of many small dislocation loops at the sidewalls of the active stripe in p/n lasers and the jagged appearance of the EL images from SI lasers point to the conditions of sidewalls as being a critical factor in this case. The near absence of dislocation loops and the comparatively smaller increase in threshold current in SI lasers which have degraded strongly suggest that strong degradation is due to a synergistic combination of residual damage in the sidewalls of the active stripe and Zn indiffusion from the p-InP:Zn current-blocking layer.

ACKNOWLEDGMENT

The authors would like to thank G. Björklund, J. Söderström, T. Carlnäs and M. Jansson for support of this work and M. Rask for clarifying discussions.

REFERENCES

[1] U. Ueda, *Reliability and Degradation of III–V Optical Devices*. Norwood. MA: Artech House, 1996.
[2] S. N. G. Chu, S. Nakahara, M. E. Twigg, L. A. Koszi, E. J. Flynn, A. K. Chin, B. P. Segner, and W. D. J. Johnston, "Defect mechanism in degradation of 1.3-μm wavelength channeled substrate buried heterostructure lasers," *J. Appl. Phys.*, vol. 63, pp. 611–623, 1988.
[3] S. N. G. Chu and S. Nakahara, "$1/2\langle 100\rangle\{100\}$ dislocation loops in zinc blende structure," *Appl. Phys. Lett.*, vol. 56, pp. 434–436, 1990.
[4] M. Fukuda, *Reliability and Degradation of Semiconductor Lasers and LEDs*. Norwood, MA: Artech House, 1991.
[5] B. C. de Cooman, C. W. T. Bulle-Lieuwma, J. A. de Poorter, and W. Nijman, "The effect of interstitial Frank partial dislocations on the gradual degradation of 1.3-μm double-channel planar buried heterostructure laser diodes," *J. Appl. Phys.*, vol. 67, pp. 3919–3926, 1990.
[6] U. Bangert, A. J. Harvey, A. R. Goodwin, and A. T. R. Briggs, "Studies of the microstructure in degraded buried heterostructure GaInAsP/InP laser diodes and its relation with the lasing threshold current," *Phys. Stat. Sol. (a)*, vol. 137, pp. 351–363, 1993.
[7] S. N. G. Chu, R. A. Logan, D. L. Coblentz, and A. M. Sergant, "Effects of excess Zn around the active-stripe mesa on the lasing threshold current of a [011] oriented InGaAsP/InP buried-heterostructure laser diode," *Appl. Phys. Lett.*, vol. 65, pp. 2377–2379, 1994.
[8] T. Kallstenius, "Sample preparation of InGaAsP/InP-based lasers for plan-view TEM using selective chemical-thinning," *J. Electrochem. Soc.*, vol. 146, pp. 758–760, 1999.
[9] J. I. Goldstein, D. E. Newbury, P. Echlin, D. C. Joy, A. D. Romig, C. E. Lyman, C. Fiori, and E. Lifshin, *Scanning Electron Microscopy and X-Ray Microanalysis*, 2nd ed. New York: Plenum, 1994.
[10] J. F. Walker, J. C. Reiner, and C. Solenthaler, "Focused ion beam sample preparation for TEM," in *Proc. Microsc. Semicond. Mater. Conf. 1995*, 1995, pp. 629–634.
[11] G. H. Olsen and T. J. Zamerowski, "Vapor-phase growth of (In, Ga)(As, P) quaternary alloys," *IEEE J. Quantum Electron.*, vol. QE-17, pp. 128–138, 1981.
[12] M. Fukuda, K. Wakita, and G. Iwane, "Observation of dark defects related to degradation in InGaAsP/InP DH lasers under accelerated operation," *Japan J. Appl. Phys.*, vol. 20, pp. L87–L90, 1981.
[13] J. W. Edington, *Practical Electron Microscopy in Materials Science*. London, U.K.: Macmillan, vol. 3, p. 27, 1976.
[14] S. O'Hara, P. W. Hutchinson, and P. S. Dobson, "The origin of dislocation climb during laser operation," *Appl. Phys. Lett.*, vol. 30, pp. 368–371, 1977.
[15] T. Matsuda, T. Namegaya, A. Kasukawa, Y. Ikegami, N. Tsukiji, T. Ijichi, and F. Iwase, "TEM observation of degraded InGaAsP MQW laser diodes," in *Proc. Microsc. Semicond. Mater. Conf. 1997*, 1997, pp. 551–556.
[16] H. Yonezu, M. Ueno, T. Kamejima, and I. Sakuma, "Lasing characteristics in a degraded GaAs-$Al_xGa_{1-x}As$ double heterostructure laser," *Japan J. Appl. Phys.*, vol. 13, pp. 835–842, 1974.
[17] P. G. Eliseev, A. G. Glebov, and M. Osinski, "Current self-distribution effect in diode lasers: Analytic criterion and numerical study," *IEEE J. Select. Topic. Quantum. Electron.*, vol. 3, pp. 499–506, 1997.
[18] L. A. Coldren and S. W. Corzine, *Diode Lasers and Photonic Integrated Circuits*. New York: Wiley, p. 38, 1995.
[19] B. Monemar, "Degradation processes in semiconductor lasers," *Physica Scripta*, vol. 24, pp. 367–374, 1981.
[20] G. P. Agrawal and N. K. Dutta, *Long-Wavelength Semiconductor Lasers*. New York: Van Nostrand Reinhold, 1986.
[21] T. Kobayashi, T. Kawakami, and Y. Furukawa, "Thermal diagnosis of dark lines in degraded GaAs-AlGaAs double-heterostructure lasers," *Japan J. Appl. Phys.*, vol. 14, pp. 508–515, 1975.
[22] D. B. Holt and D. C. Joy, *SEM Microcharacterization of Semiconductors*. Oxford, U.K.: Academic, p. 246, 1989.
[23] D. Wittorf, A. Rucki, W. Jäger, R. H. Dixon, K. Urban, H.-G. Hettwer, N. A. Stolwijk, and H. Mehrer, "Evidence of point defect supersaturation during Zn diffusion in InP single crystals," *J. Appl. Phys.*, vol. 77, pp. 2843–2845, 1995.
[24] Y. Kondo, K. Kishi, M. Itoh, H. Oohashi, Y. Itaya, and M. Yamamoto, "1.3-μm buried-heterostructure lasers using a CH_4 reactive-ion-etched mesa structure grown by metalorganic vapor phase epitaxy," in *Proc. 8th Int. Conf. on InP and Related Materials*, 1996, pp. 384–387.
[25] H. Oohashi, M. Fukuda, Y. Kondo, M. Wada, Y. Tohmori, Y. Sakai, H. Toba, and Y. Itaya, "Reliability of 1300-nm spot-size converter integrated laser diodes for low-cost optical modules in access networks," *J. Lightwave Technol.*, vol. 16, pp. 1302–1306, 1998.

Thomas Kallstenius, photograph and biography not available at the time of publication.

Jakob Bäckström, photograph and biography not available at the time of publication.

Ulf Smith, photograph and biography not available at the time of publication.

Björn Stoltz, photograph and biography not available at the time of publication.

Authorized licensed use limited to: Univ of Calif Santa Barbara. Downloaded on November 29, 2009 at 10:34 from IEEE Xplore. Restrictions apply.